Hindawi
Mathematical Problems in Engineering
Volume 2020, Article ID 1580297, 11 pages
https://doi.org/10.1155/2020/1580297

Research Article

Modeling and Analysis of a Hydraulic Energy-Harvesting Shock Absorber

Zhifei Wu and Guangzhao Xu

School of Mechanical and Vehicle Engineering, Taiyuan University of Technology, Taiyuan 030024, China

Correspondence should be addressed to Zhifei Wu; wuzhifei@tyut.edu.cn

Received 5 November 2019; Revised 30 December 2019; Accepted 16 January 2020; Published 8 February 2020

Academic Editor: Fausto Arpino

Copyright © 2020 Zhifei Wu and Guangzhao Xu. This is an open access article distributed under the Creative Commons Attribution License, which permits unrestricted use, distribution, and reproduction in any medium, provided the original work is properly cited.

This paper proposes a hydraulic energy-harvesting shock absorber prototype, which realizes energy harvesting of the vibration energy dissipated by the automobile suspension system. The structural design of the proposed shock absorber ensures that the unidirectional flow of oil drives the hydraulic motor to generate electricity while obtaining an asymmetrical extension/compression damping force. A mathematical model of the energy-harvesting shock absorber is established, and the simulation results indicate that the damping force can be controlled by varying the load resistance of the feed module, thus adjusting the required damping force ratio of the compression and recovery strokes. By adjusting the external load, the target indicator performance of the shock absorber is achieved while obtaining the required energy recovery power. A series of experiments are conducted on the prototype to verify the validity of the damping characteristics and the energy recovery efficiency as well as to analyze the effect of external load and excitation speed on these characteristics.

1. Introduction

Recovery of energy dissipated during driving of automobiles has been extensively researched [1, 2]. In addition to brake energy recovery, suspension energy recovery technology has been gradually implemented in vehicles. A hydraulic energy-harvesting shock absorber can convert vibration energy dissipated by the suspension system into electric energy for recycling, thereby realizing energy conservation and ensuring a stable working performance of the shock absorber. Therefore, it has received considerable research attention.

Many types of energy-harvesting shock absorbers have been developed. Salman presented a regenerative absorber based on helical gears and dual tapered roller clutches for electric vehicles [3]. Zhang presented an energy-harvesting shock absorber that uses an arm-teeth mechanism to convert linear motion to rotational motion and to amplify the generator input speed [4]. Energy-harvesting dampers are of two main forms: electromagnetic and electrohydraulic. Zuo et al. designed and established a 1 : 2 prototype based on a linear motor-type feed-through suspension [5]. Zheng et al. researched the structure of feed suspension with a DC motor and a ball screw mechanism and improved the performance of the suspension system of the vehicle by the active control of vibration energy [6, 7]. Li et al. proposed a novel energy-harvesting variable/constant damping suspension system with a motor-based electromagnetic damper, which can simultaneously achieve energy recovery and storage as well as adjust the damping force according to different road conditions [8]. Similarly, various hydraulic-electric energy-harvesting suspension systems have been used in the oil circuit system design to convert the reciprocating vibration energy of the piston into the hydraulic energy of the damping oil, thus facilitating the rotation of the hydraulic motor in the driving system and driving the generator to generate electricity [9–11]. However, the damping fluid in an oil circuit system frequently switches the flow direction due to the nonuniform excitation caused by uneven road surfaces, which dramatically reduces the feed efficiency of the generator. Fang conducted considerable research on hydraulic-electric energy-feeding suspension and proposed several implementation schemes by establishing dynamic

models and simulation analysis. A bench test of the prototype was conducted for more systematic research [12–14]. Fang et al. also studied the effect of road excitation frequency, external load, and damping coefficient on energy recovery efficiency [15]. Many research studies on energy-harvesting shock absorbers mainly focused on road tests and the effect of these shock absorbers on vehicle dynamics. Abdelkareem et al. summarized the current situation of energy-harvesting dampers mainly from four aspects, namely, the principle, simulation, a bench test, and a road test, and summarized the advantages and limitations of energy-harvesting dampers [16]. Zou et al. proposed a hydraulic interconnected suspension system based on a hydraulic energy-regenerative shock absorber and investigated the dynamic characteristics of the system based on a 4-degrees-of-freedom (DOF) longitudinal half-vehicle model [17]. Zou et al. also investigated different working modes, including bounce, pitch, and roll, of the damper and compared the damper with conventional shock absorbers in terms of suspension dynamics and energy recovery [18]. Abdelkareem et al. established a comprehensive simulation model to analyze the potential harvested power of vehicles of different models and for different standard driving cycles [19]. They also used the HAVAL H8 SUV model to conduct real-vehicle road tests to analyze and verify the potential harvested power [20]. Abdelkareem et al. analyzed the potential energy recovery of suspension systems in different driving environments for six types of heavy trucks [21]. Wu et al. studied the effect of parameters of the accumulator on a hydraulic system and provided useful guidelines for the selection of system component parameters [22]. The aforementioned studies mainly aimed at conducting road tests to determine the corresponding efficiency of recovery power and lack a detailed analysis of the recovery power of the damper and the factors affecting the recovery efficiency.

The main objectives of the present study are as follows: (1) To design a hydraulic energy-harvesting shock absorber prototype that can achieve unidirectional oil flow that drives the hydraulic motor to generate electricity. (2) To propose a method for adjusting the damping ratio and to obtain an asymmetric damping ratio through the design structure. (3) To construct a model of the energy-harvesting shock absorber and to analyze and refine the factors affecting the energy recovery power and efficiency as well as determine the extent to which the different factors affect them.

2. Working Principle of the Energy-Harvesting Shock Absorber

The principle of the hydraulic energy-harvesting shock absorber is depicted in Figure 1. It consists of a double-acting hydraulic cylinder, a hydraulic rectifier comprising two check valves, an accumulator, a hydraulic motor, a permanent magnetic generator, and hydraulic lines. In this study, the upward and downward motions of the piston are described as compression and extension, respectively. In the compression stroke, the oil directly flows through check valve 1 to supplement the rod-end chamber; the oil flow rate through the hydraulic motor is obtained by multiplying the rod area and piston speed. In the extension stroke, the oil flow rate through the hydraulic motor is obtained by multiplying the annular area of the piston and piston speed. The fuel flow drives the generator to generate electricity. By this design principle, the damping force of the compression stroke is mainly generated from check valve 1, while the damping force of the extension stroke is primarily generated from the hydraulic motor and check valve 2. This allows adjustment of the relevant component parameters separately to achieve the required compression and extension damping forces.

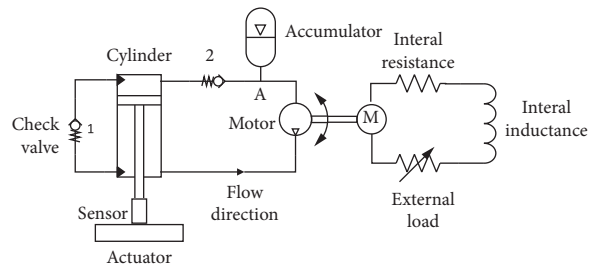

Figure 1: Schematic diagram of the hydraulic energy-harvesting shock absorber.

As shown in Figure 1, in the compression stroke, because check valve 2 is in the closed state, the oil directly flows through check valve 1 to supplement the rod-end chamber. Because the volume of the rod-end chamber is lower than that of the cap-end chamber, the oil will flow through the hydraulic motor and lead to generation of electricity. When the hydraulic motor reaches node A, owing to the high pressure at the left end of check valve 2, which is in the closed state, some part of the oil is stored in the accumulator. In the extension stroke, the downward movement of the piston drives the oil in the rod-end chamber to be completely discharged. Because check valve 1 is in the closed state, the oil can only pass through the hydraulic motor. After the oil-driven hydraulic motor generates electricity, the oil flows back to the cap-end chamber together with the oil stored in the accumulator during the compression stroke. According to this working principle, the overall damping force of the energy-harvesting damper can be divided into inherent damping force and controllable damping force. Inherent damping is caused by the no-load rotational damping force of the energy-feeding module and the passive damping of the accumulator, oil line, and check valve in the actuator. The controllable damping force refers to the hydraulic motor damping force caused by the generator's counter electromotive force.

3. Mathematical Model

3.1. Flow Rate Analysis. According to the principle analysis, the extension stroke flow rate is

$$Q_{\mathrm{pi}} = Q_{\mathrm{pu}} = A_c v(t), \tag{1}$$

$$Q_{v1} = 0, \tag{2}$$

$$Q_{v2} = A_g v(t). \tag{3}$$

The compression stroke flow is

$$Q_{v1} = \left|A_g v(t)\right|, \tag{4}$$

$$Q_{\mathrm{pi}} = Q_{\mathrm{pu}} = \left|A_r v(t)\right|, \tag{5}$$

$$Q_{v2} = 0, \tag{6}$$

where Q_{pi} and Q_{pu} are the flow rates through the hydraulic line and the pump, respectively; Q_{v1} and Q_{v2} are the flow rates through check valves 1 and 2, respectively; A_c is the annular area of the piston; $v(t)$ is the speed of the piston movement; A_g is the full piston face area; and A_r is the piston rod area.

The relationship between hydraulic motor speed and torque is as follows:

$$\omega_{\mathrm{pu}} = \frac{2\pi Q_{\mathrm{pu}}}{q}\eta_v, \tag{7}$$

$$T_{\mathrm{pu}} = \frac{\Delta P_{\mathrm{pu}} q}{2\pi}\eta_m, \tag{8}$$

where ω_{pu} is the rotating speed of the hydraulic motor, T_{pu} is the torque of the hydraulic motor, Q_{pu} is the flow rate through the hydraulic motor, and q is the motor displacement. ΔP_{pu} is the pressure difference between the inlet and outlet oil in the hydraulic motor, η_v is the volumetric efficiency of the hydraulic motor, and η_m is the mechanical efficiency of the hydraulic motor.

When the hydraulic motor drives the generator to rotate through the coupling, the relationship of the generator output voltage U_{emf} and the generator drive torque T_g is as follows:

$$U_{\mathrm{emf}} = k_e \omega_g, \tag{9}$$

$$T_g = J_g \frac{\mathrm{d}\omega}{\mathrm{d}t} + k_t I, \tag{10}$$

where ω_g is the generator rotating speed, k_e and k_t are the generator's counter electromotive force constant and torque constant, respectively, J_g is the inertia of the generator rotor, and I is the generator output current.

According to Kirchhoff's voltage law, the following relationship can be obtained:

$$U_{\mathrm{emf}} - L_{\mathrm{in}} \frac{\mathrm{d}I}{\mathrm{d}t} - I\left(R_{\mathrm{in}} + R_{\mathrm{ex}}\right) = 0, \tag{11}$$

where L_{in} is the generator internal inductance, R_{in} is the generator internal resistance, (usually the internal inductance of the generator is negligible), and R_{ex} is the external generator load.

Since the hydraulic motor and the generator are connected by the coupling, we have

$$\omega_{\mathrm{pu}} = \omega_g, \tag{12}$$

$$T_{\mathrm{pu}} = T_g. \tag{13}$$

Based on equations (7)–(13), the hydraulic pressure difference ΔP_{pu} between the hydraulic motor inlet and outlet in terms of the flow rate Q_{pu} of the oil flowing through the hydraulic motor can be obtained as follows:

$$\Delta P_{\mathrm{pu}} = \frac{4\pi^2 J_g \eta_v}{q^2 \eta_m}\dot{Q}_{\mathrm{pu}} + \frac{4\pi^2 k_t k_e \eta_v}{q^2 \eta_m \left(R_{\mathrm{in}} + R_{\mathrm{ex}}\right)} Q_{\mathrm{pu}}. \tag{14}$$

3.2. Controllable Damping Force. Equation (14) indicates that when the external load R_{ex} is infinite, the hydraulic motor works with inherent damping. The second term on the right side of the formula implies that the hydraulic motor can be controlled by an external load. The pressure decrease can be expressed as follows:

$$\Delta P_{\mathrm{pc}} = \frac{4\pi^2 k_t k_e \eta_v}{q^2 \eta_m \left(R_{\mathrm{in}} + R_{\mathrm{ex}}\right)} Q_{\mathrm{pu}} = k_{\mathrm{pc}} Q_{\mathrm{pu}}, \tag{15}$$

where k_{pc} is the equivalent controllable impedance of the feed module and is affected by the displacement of the hydraulic motor, mechanical efficiency, volumetric efficiency, and power generation characteristics of the generator.

In this part, only the controllable pressure decrease is considered, which is applied to the two ends of the actuator piston, and the equivalent controllable damping force of the energy-absorbing damper can be obtained. The following relationship is satisfied in the extension stroke:

$$P_{\mathrm{upc}} = 0, \tag{16}$$

$$P_{\mathrm{downc}} = \Delta P_{\mathrm{pc}}, \tag{17}$$

where p_{upc} and P_{downc} represent the controllable pressures of the rod-end and cap-end chambers, respectively.

The compression stroke satisfies the following relationship:

$$P_{\mathrm{upc}} = \Delta P_{\mathrm{pc}}, \tag{18}$$

$$P_{\mathrm{downc}} = \Delta P_{\mathrm{pc}}. \tag{19}$$

Combining equations (1)–(6) and (16)–(19), the total equivalent controllable damping force of the hydraulic energy-absorbing damper can be expressed as follows:

$$\begin{aligned} F_{\mathrm{sa}} &= A_c P_{\mathrm{downc}} - A_g P_{\mathrm{upc}} \\ &= \frac{\pi^3 k_t k_e \eta_v \left(D^2 - d_{\mathrm{rod}}^2\right)^2 v(t)}{q^2 \eta_m \left(R_{\mathrm{in}} + R_{\mathrm{ex}}\right)}, \quad v(t) \geq 0 \\ &= \frac{\pi^3 k_t k_e \eta_v d_{\mathrm{rod}}^4 v(t)}{q^2 \eta_m \left(R_{\mathrm{in}} + R_{\mathrm{ex}}\right)}, \quad v(t) \leq 0. \end{aligned} \tag{20}$$

Furthermore, based on equations (9)–(13), the expression of the feed power is

$$P_r = I^2 R_{\text{ex}} = \frac{\pi^4 k_e^2 \eta_v^2 \left(D^2 - d_{\text{rod}}^2\right)^2 R_{\text{ex}}}{4q^2 \left(R_{\text{in}} + R_{\text{ex}}\right)^2} v^2(t), \quad v(t) \geq 0$$

$$= \frac{\pi^4 k_e^2 \eta_v^2 d_{\text{rod}}^4 R_{\text{ex}}}{4q^2 \left(R_{\text{in}} + R_{\text{ex}}\right)^2} v^2(t), \quad v(t) \leq 0. \tag{21}$$

The above equations indicate that, in the case where the mechanical structural parameters are determined, the magnitude of feed power of the compression stroke and the recovery stroke depends mainly on the excitation speed and the magnitude of the load resistance.

3.3. Inherent Damping Force

(1) Calculation of the pressure decrease of the no-load motor

According to the motor pressure decrease formula, when the external resistor is infinite, the relationship of the hydraulic pressure decrease between the hydraulic motor inlet and outlet with the flow rate under the no-load conditions is given as follows:

$$\Delta P_{\text{pup}} = \frac{4\pi^2 J_g \eta_v}{q^2 \eta_m} \dot{Q}_{\text{pu}} = c_{\text{pp}} \dot{Q}_{\text{pu}}, \tag{22}$$

where ΔP_{pup} and Q_{pu} represent the pressure difference between the hydraulic motor inlet and outlet oil and the hydraulic motor flow rate, respectively; c_{pp} is the equivalent inherent damping of the feed module.

(2) Hydraulic line pressure decrease calculation

Hydraulic line pressure decrease ΔP_{pi} can be expressed as

$$\Delta p_{\text{pi}} = \frac{128 \rho L_{\text{pi}} \mu}{\pi d_{\text{pi}}^4} Q_{\text{pi}} = k_{\text{pi}} Q_{\text{pi}}, \tag{23}$$

where ρ represents the oil density; k_{pi} is the pipeline pressure decrease coefficient; Q_{pi} is the oil flow rate through the pipeline; L_{pi} and d_{pi} are the hydraulic pipe length and diameter, respectively; and μ is the dynamic viscosity of the oil.

(3) Check valve pressure decrease calculation

When the oil flows through the check valve, the pressure at the check valve decreases, which is obtained by the orifice formula:

$$\Delta P_{\text{vi}} = \left(\sqrt{\frac{\rho}{2}} \frac{K_{\text{vi}}}{C_d B_{\text{vi}} A_{\text{vi}}} Q_{\text{vi}}\right)^{2/3}, \tag{24}$$

where Q_{vi} represents the flow rate through the check valve i, $i = 1, 2$; ΔP_{vi} is the check valve inlet and outlet pressure difference; C_d is the flow coefficient; B_{vi}, A_{vi}, and K_{vi} are the valve blade perimeter, area, and stiffness, respectively, of the check valve i.

(4) Accumulator

Because of the fixed mass of gas in the accumulator, according to the properties of an ideal gas, the relationship between the volume and pressure of the gas is given by

$$P_0 V_0^n = P_t V_t^n, \tag{25}$$

where P_0 and V_0 represent the gas pressure and volume in the accumulator in the initial state, respectively; P_t and V_t are the gas pressure and volume in the accumulator at t time, respectively; and n is the variable index. The relationship between the gas volume at t time V_t and the initial gas volume V_0 is

$$V_t - V_0 = A_r \int v(t) dt. \tag{26}$$

Based on equations (25) and (26), the gas pressure in the accumulator at time t is given by

$$P_t = \frac{P_0 V_0^n}{V_t^n} = \frac{P_0 V_0^n}{\left(A_r \int v(t) dt + V_0\right)^n}, \tag{27}$$

where P_{downp} and P_{upp} are the hydraulic oil pressure of the rod-end and cap-end chambers, respectively, under a no-load condition. The extension stroke satisfies the following relationship:

$$P_{\text{upp}} = P_t - \Delta P_{v2}, \tag{28}$$

$$P_{\text{downp}} = \Delta P_{\text{pup}} + P_t + \Delta P_{\text{pi}}. \tag{29}$$

The compression stroke satisfies the following relationship:

$$P_{\text{upp}} = \Delta P_{\text{pup}} + P_t + \Delta P_{\text{pi}} + \Delta P_{v1}, \tag{30}$$

$$P_{\text{downp}} = \Delta P_{\text{pup}} + P_t + \Delta P_{\text{pi}}. \tag{31}$$

Combining equations (1)–(6) and (28)–(31), the total inherent damping force of the hydraulic energy-harvesting shock absorber, F_p, can be expressed as

$$\begin{aligned} F_p &= A_c P_{\text{downp}} - A_g P_{\text{upp}} = A_c \left(\Delta P_{\text{pup}} + P_t + \Delta P_{\text{pi}}\right) \\ &\quad - A_g \left(P_t - \Delta P_{v2}\right), \quad v(t) \geq 0 \\ &= A_c \left(\Delta P_{\text{pup}} + P_t + \Delta P_{\text{pi}}\right) \\ &\quad - A_g \left(\Delta P_{\text{pup}} + P_t + \Delta P_{\text{pi}} + \Delta P_{v1}\right), \quad v(t) \leq 0, \end{aligned} \tag{32}$$

which is

$$F_p = -\frac{\pi P_0 V_0^n d_{\text{rod}}^2}{4\left(V_0 + \pi/4 d_{\text{rod}}^2 \int v(t)\mathrm{d}t\right)^n} + \frac{32\rho L_{\text{pi}}\mu}{d_{\text{pi}}^4}\left(D^2 - d_{\text{rod}}^2\right)^2 v(t) + \frac{\pi}{8}\rho^{1/3}\left(\frac{K_{v2}}{C_d d_{v2} A_{v2}}\right)^{2/3} D^{11/3} v(t)^{2/3}, \quad v(t) \geq 0$$

$$= -\frac{\pi P_0 V_0^n d_{\text{rod}}^2}{4\left(V_0 + \pi/4 d_{\text{rod}}^2 \int v(t)\mathrm{d}t\right)^n} - \frac{32\rho L_{\text{pi}}\mu}{d_{\text{pi}}^4} d_{\text{rod}}^4 v(t) - \frac{\pi}{8}\rho^{1/3} \cdot \left(\frac{K_{v2}}{C_d d_{v2} A_{v2}}\right)^{2/3} D^{11/3} v(t)^{2/3}, \quad v(t) \leq 0. \tag{33}$$

3.4. Overall Damping Force. Combining equations (16)–(19) and (28)–(31), the hydraulic oil pressure can be expressed as

$$P_{\text{down}} = P_{\text{downp}} + P_{\text{downc}}, \tag{34}$$

$$P_{\text{up}} = P_{\text{upp}} + P_{\text{upc}}, \tag{35}$$

where P_{up} and P_{down} are the hydraulic oil pressures of the rod-end and cap-end chambers.

According to the above analysis, the extension stroke satisfies the following relationship:

$$P_{\text{down}} = \Delta P_{\text{pu}} + P_t + \Delta P_{\text{pi}}, \tag{36}$$

$$P_{\text{up}} = P_t - \Delta P_{v2}. \tag{37}$$

The compression stroke satisfies the following relationship:

$$P_{\text{down}} = \Delta P_{\text{pu}} + P_t + \Delta P_{\text{pi}}, \tag{38}$$

$$P_{\text{up}} = \Delta P_{\text{pu}} + P_t + \Delta P_{\text{pi}} + \Delta P_{v1}. \tag{39}$$

According to equations (1)–(6) and (36)–(39), the overall damping force F is as follows:

$$F = A_c P_{\text{down}} - A_g P_{\text{up}} = -\frac{\pi P_0 V_0^n d_{\text{rod}}^2}{4\left(V_0 + (\pi/4) d_{\text{rod}}^2 \int v(t)\mathrm{d}t\right)^n} + \left(\frac{32\rho L_{\text{pi}}\mu}{d_{\text{pi}}^4} + \frac{\pi^3 k_t k_e \eta_v}{q^2 \eta_m \left(R_{\text{in}} + R_{\text{ex}}\right)}\right)\left(D^2 - d_{\text{rod}}^2\right)^2 v(t) + \frac{\pi}{8}\rho^{1/3}\left(\frac{K_{v2}}{C_d d_{v2} A_{v2}}\right)^{2/3} D^{11/3} v(t)^{2/3}, \quad v(t) \geq 0$$

$$= -\frac{\pi P_0 V_0^n d_{\text{rod}}^2}{4\left(V_0 + (\pi/4) d_{\text{rod}}^2 \int v(t)\mathrm{d}t\right)^n} - \left(\frac{32\rho L_{\text{pi}}\mu}{d_{\text{pi}}^4} + \frac{\pi^3 k_t k_e \eta_v}{q^2 \eta_m \left(R_{\text{in}} + R_{\text{ex}}\right)}\right) d_{\text{rod}}^4 v(t) - \frac{\pi}{8}\rho^{1/3}\left(\frac{K_{v2}}{C_d d_{v2} A_{v2}}\right)^{2/3} D^{11/3} v(t)^{2/3}, \quad v(t) \leq 0. \tag{40}$$

4. Simulation and Analysis of the Damping Force and Feed Power

4.1. Damping Controllable Characteristics of the Energy-Harvesting Damper. According to the theoretical analysis of the hydraulic energy-harvesting damper, the damping force of the damper is affected by the excitation frequency and external load. Therefore, this section presents a simulation study on the controllable range of the damping force under the same excitation amplitude (50 mm), different excitation frequencies, and different external loads. We established a mathematical model and set simulation parameters for an excitation amplitude of 50 mm. The external load resistance was set to 10 Ω, 30 Ω, 50 Ω, and 100 Ω. The damper characteristics under different excitation frequencies and external load resistance are shown in Figure 2.

Figure 2 shows that the damping force of the extension stroke is larger than that of the compression stroke, which is consistent with the requirement of asymmetric damping characteristics for conventional dampers. As the load increases, both extension and compression stroke damping forces increase, and the extension stroke is relatively obvious. At the same frequency and under the same change in load resistance, the extension stroke damping force can be adjusted from −583 N to −1023 N in multiples of 1.75 at 0.23 Hz. The extension stroke damping force can be adjusted from −2210 N to −3393 N in multiples of 1.54 at 0.62 Hz. Note that, as the frequency increases, the adjustable range of the damping force widens and the adjustable multiple decreases. The accumulator parameters greatly affect the damping force in both compression and extension strokes. In the first half of the compression stroke, the damping force increases gradually due to the accumulator energy storage. In the second half of the extension stroke, the impact and magnitude of the force caused by the accumulator pressure release are related to the frequency. The damping force in the second half of the extension stroke at 0.23 Hz is larger than that in the first half.

4.2. Simulation Analysis of the Effect of the Hydraulic Energy-Harvesting Shock Absorber on Vehicle Suspension Dynamics.

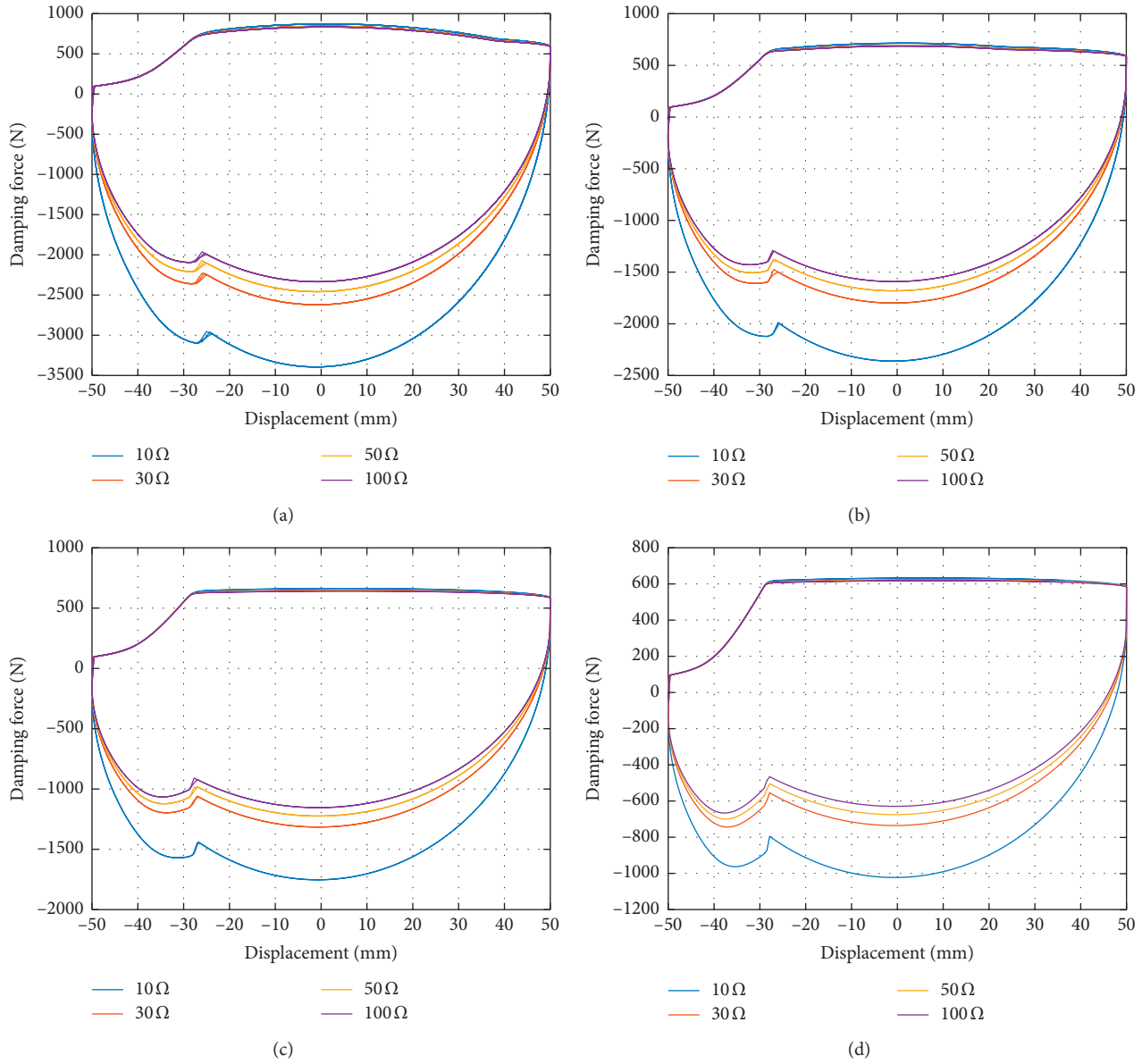

Figure 2: Load resistance characteristics at an excitation frequency of 0.62 Hz (a), 0.45 Hz (b), 0.35 Hz (c), and 0.23 Hz (d).

To analyze the effect of the damping characteristics of the shock absorber on the vehicle suspension dynamics, we established a 2-DOF quarter car model in MATLAB/Simulink. Then, the results of the comparison and analysis of sprung mass acceleration in Figure 3, suspension deflection response, and tire load response indicate that the effect of the hydraulic energy-harvesting shock absorber is less on the vehicle dynamic performance during energy recovery.

4.3. Effect of External Load on the Energy Recovery Characteristics of the Hydraulic Energy-Harvesting Shock Absorber. According to the theoretical analysis of the energy-absorbing damper, the feed energy of the damper is affected by the excitation frequency and the external load. The simulation settings for this analysis are the same as those for the analysis in the previous section. We discuss the factors that affect the energy recovery power and efficiency under the same excitation amplitude (50 mm), different excitation speeds, and different external loads.

From equations (21) and (40), the energy recovery efficiency η_h is obtained as

$$\eta_h = \frac{P_r}{Fv(t)}. \tag{41}$$

Because the recovery power of the compression stroke is extremely small, we mainly focus on the extension stroke. Consider P_r as the peak recovery power of the extension stroke, F is the peak damping force of the extension stroke, and $v(t)$ is the peak excitation speed at the excitation frequency to obtain the corresponding energy recovery efficiency. Figures 4 and 5 indicate that, as the excitation frequency increases and the external load resistance

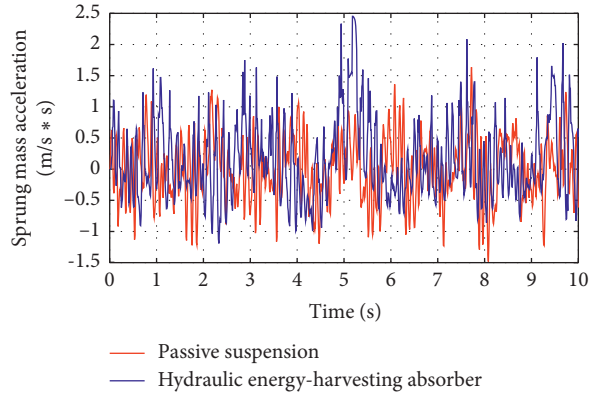

Figure 3: Sprung mass acceleration of the hydraulic energy-harvesting absorber and passive suspension.

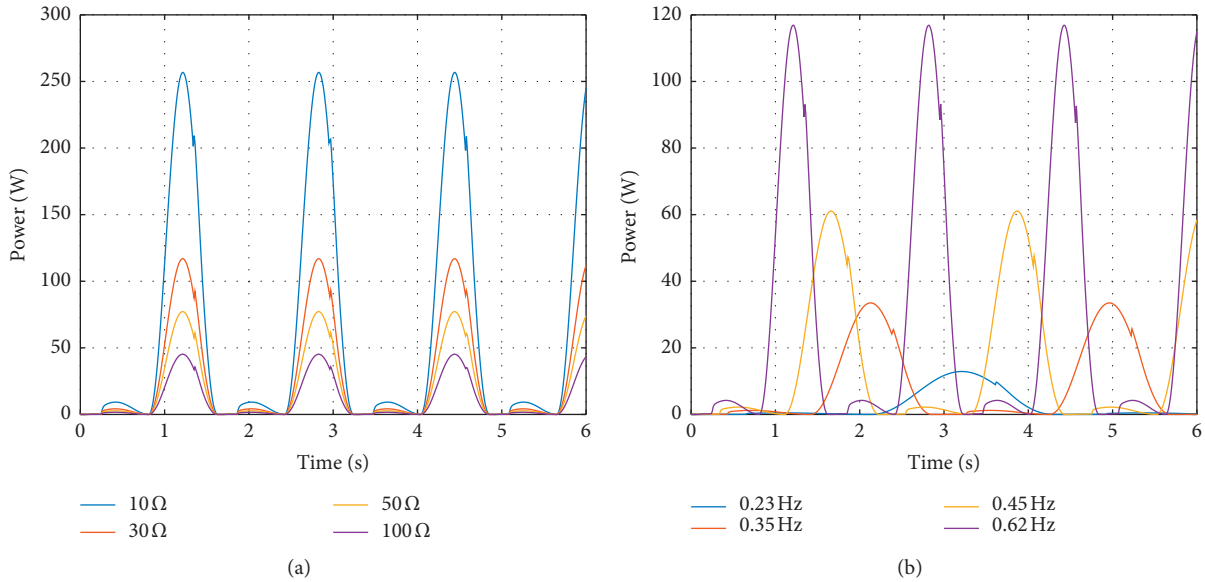

Figure 4: Feed power (a) under different loads at an excitation frequency of 0.62 Hz and (b) at different frequencies for a load of 30 Ω.

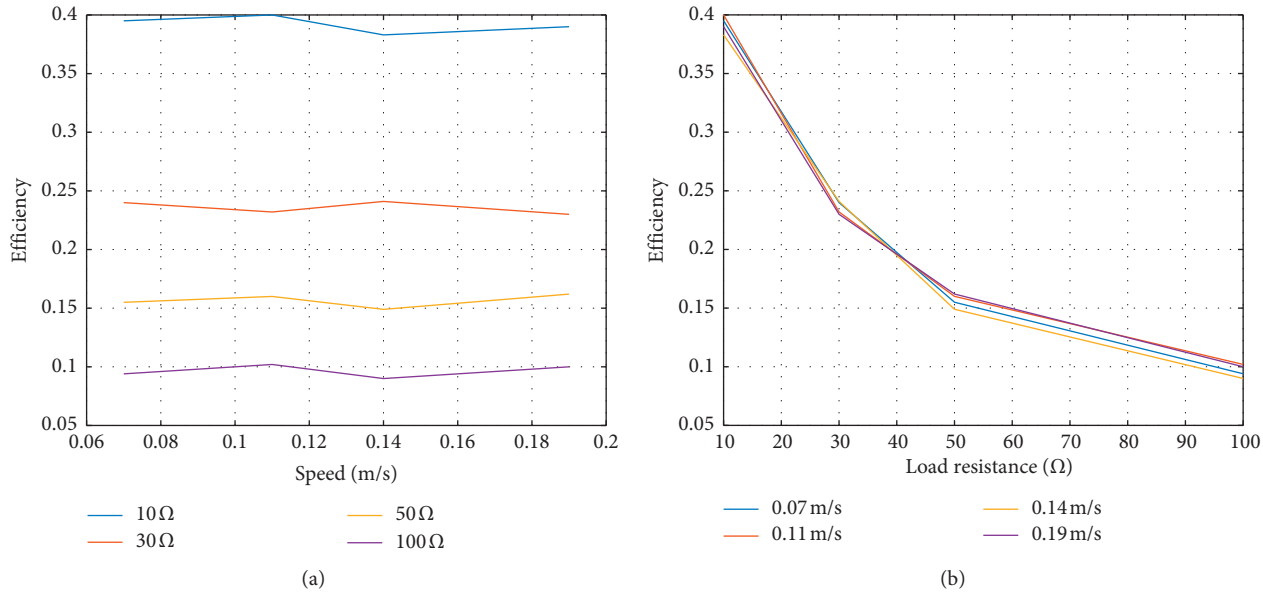

Figure 5: Feed efficiency (a) under different load resistance and (b) different excitation speeds.

decreases, the feed power increases greatly. In the first half of the compression stroke, the feed power is extremely small due to the energy storage of the accumulator, and there is a sudden change in power during the extension stroke. The excitation frequency has little effect on the energy efficiency. As the speed increases, the feed efficiency basically remains unchanged. As the load resistance decreases, the feed efficiency increases considerably.

4.4. External Load and Feed Efficiency Corresponding to Target Indicator Characteristics. Through simulation, a hydraulic cylinder diameter of 50 mm was selected such that the standard specifications under the conventional excitation (input frequency 1.655 Hz and amplitude 50 mm) are met. The maximum extension and compression damping force that the damper needs to provide are −7000 N and 2800 N, respectively. During the simulation process, the load value was changed several times, and the load resistance value and the corresponding feed power value under the target indicator characteristic were obtained.

Figure 6 shows that when the external load was 53 Ω, the maximum extension and compression damping force reached −6972 N and 2768 N, respectively, which basically meets the target damping requirement. At the same time, the peak power can be recovered at 505.52 W, and the feed efficiency is 14.5%.

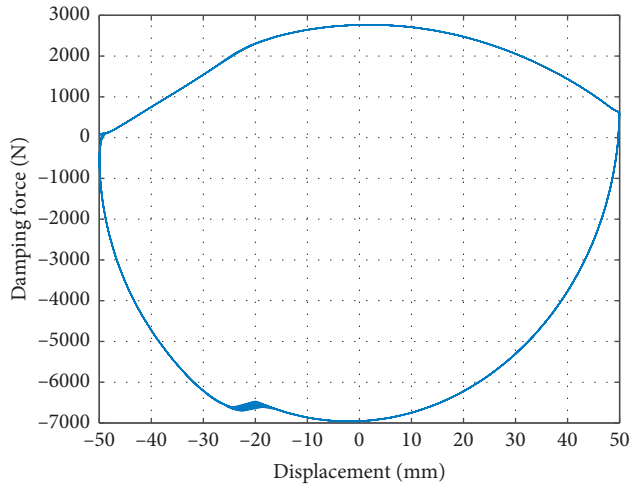

Figure 6: Damping force diagram under target indicator characteristics.

5. Experimental Methodologies

5.1. Experimental Setup. To evaluate the effects of different excitation speeds and external loads on feed energy dampers, a test bench was built, and an existing hydraulic excitation platform was used to simulate road excitation. As shown in Figure 7, the test bench is mainly composed of a double-acting hydraulic cylinder, check valves, an accumulator, a hydraulic motor, a generator, a high-power sliding rheostat, and a compression and tension load sensor.

The theory analysis and simulation described in previous sections show that the damping force of the shock absorber is affected by the excitation frequency and external load. Therefore, the damping force at a constant excitation displacement, different excitation velocities, and different external loads was experimentally studied. Because the excitation platform used in the experiment cannot provide sinusoidal excitation, the experiment adopted uniform excitation, and the maximum speed of the sinusoidal excitation is the same as the experimental excitation speed under the simulation condition. The experimental parameter setting is shown in Table 1.

5.2. Experimental Procedure. The hydraulic excitation platform was adjusted to vary the excitation speed, and the sliding rheostat was adjusted to vary the external load for the orthogonal test. The value of the compression and tension load from the sensor and the voltage value across the sliding rheostat were collected using a data acquisition instrument, which will be detailed as follows.

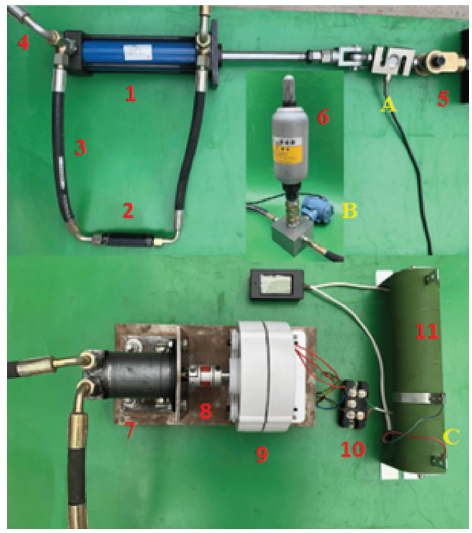

Figure 7: Key components of the energy-harvesting shock absorber system: (1) hydraulic cylinder, (2, 4) check valves, (3) hose, (5) hydraulic excitation platform, (6) accumulator, (7) hydraulic motor, (8) coupling, (9) three-phase alternator, (10) rectifier, (11) sliding rheostat, (A) force transductor, (B) pressure transductor, and (C) voltage transductor.

Table 1: Main component parameters of the hydraulic excitation system.

Parameters	Value				Unit
External load	10	30	50	100	Ω
Displacement	±50				mm
Speed	0.19	0.14	0.11	0.07	m/s
Frequency	0.62	0.45	0.35	0.23	Hz

5.3. Data Acquisition. In this study, an INV3060A 16-channel data acquisition instrument was used for collecting data. The DYLY-103 load cell was used as the compression and tension load sensor. During the experiment, a DASP

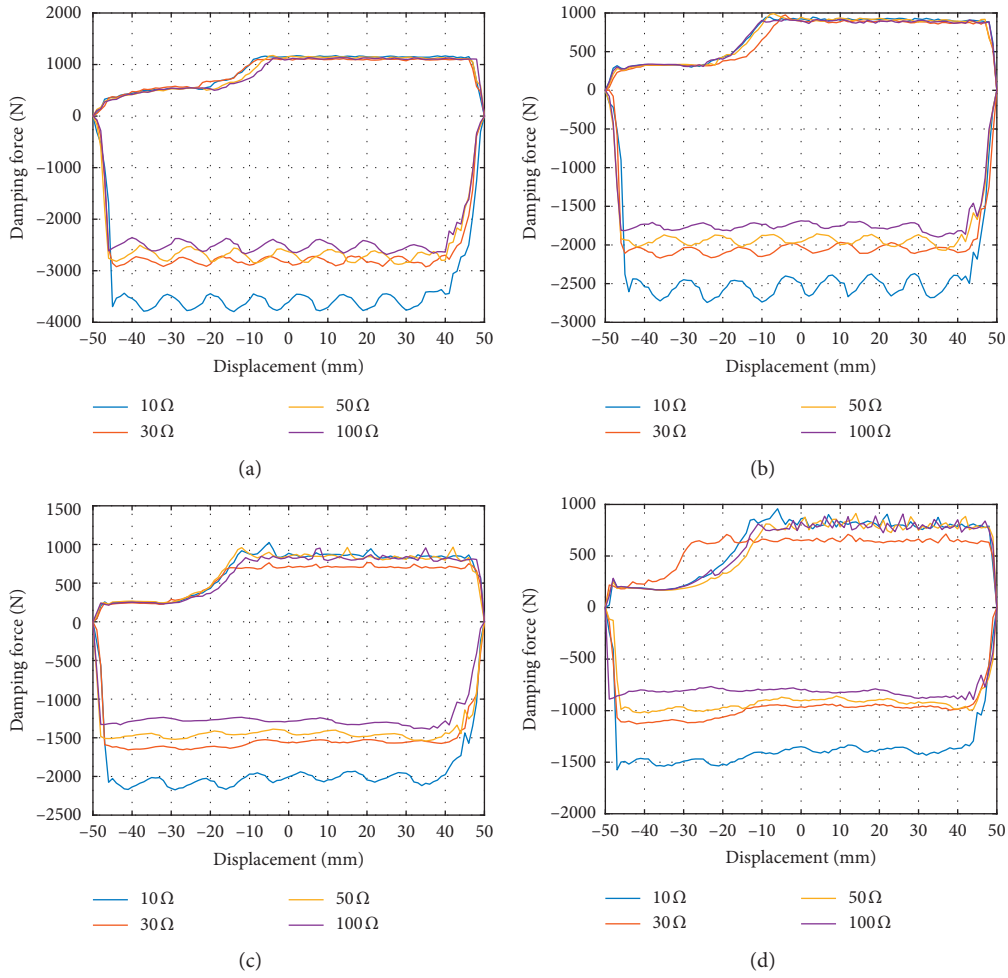

Figure 8: Damping characteristics with different loads at an excitation speed of 0.19 m/s (a), 0.14 m/s (b), 0.11 m/s (c), and 0.07 m/s (d).

system was used to collect and display the values from the compression and tension load sensor and the sliding varistor voltage.

6. Results and Discussion

6.1. Damping Controllable Feature Verification. This section discusses the results of the experimental study on the controllable range of the damping force under the same excitation amplitude (50 mm), different excitation speeds, and different external loads.

Figure 8 indicates that, in the test data, the damping force of the extension stroke was larger than that of the compression stroke, which is consistent with the requirement of asymmetric damping characteristics for conventional shock absorbers. Thus, the established model is verified by both experimental and simulation results. However, the experimental data were higher than the simulation data. This is because the simulation is based on ideal conditions, whereas in actual conditions, due to the low oil temperature, a certain energy loss occurred in pipe joints and the flow meter. We can observe that, as the excitation speed increased, under the same load change condition, the adjustable range of the damping force increased, with decreasing adjustable multiple. The accumulator significantly affected the damping force in both compression and extension strokes. In the first half of the compression stroke, the damping force increased gradually due to the accumulator energy storage. In the second half of the extension stroke, the impact and magnitude of the force caused by the accumulator pressure release were dependent on frequency. It can be seen that the damping force in the second half of the extension stroke at 0.073 m/s was greater than that in the first half. In addition, because there were a large number of pipe joints and other factors affecting the line pressure decrease during the actual test, the response speed of the extension stroke accumulator under the test conditions was much slower than that in the simulation conditions.

6.2. Verification of the Effect of External Load on Feed Characteristics. To calculate the energy recovery power and efficiency, the average values of the damping force and generation voltage near the midpoint of the displacement of the extension stroke were taken as the effective values of the damping force and voltage.

From Figures 9 and 10, the following observations can be inferred: (1) The test and simulation results are consistent;

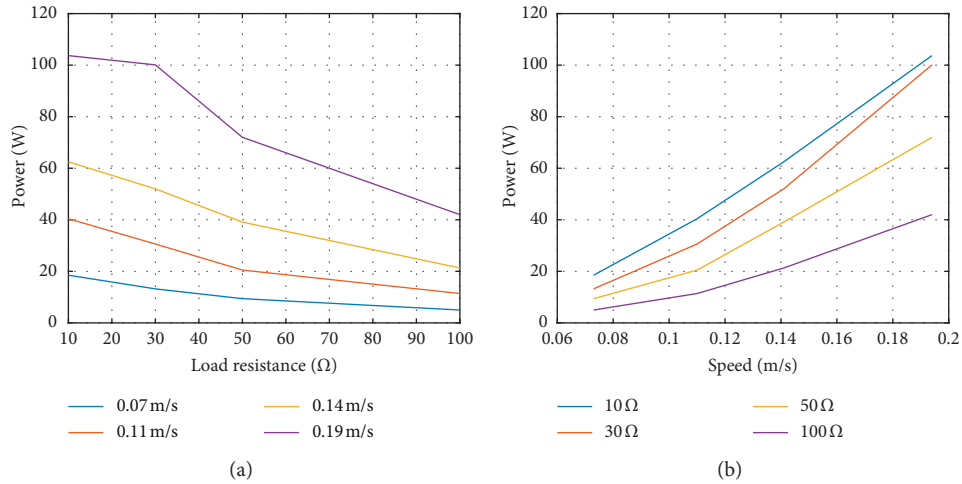

Figure 9: Variation of power with (a) speed and (b) load resistance.

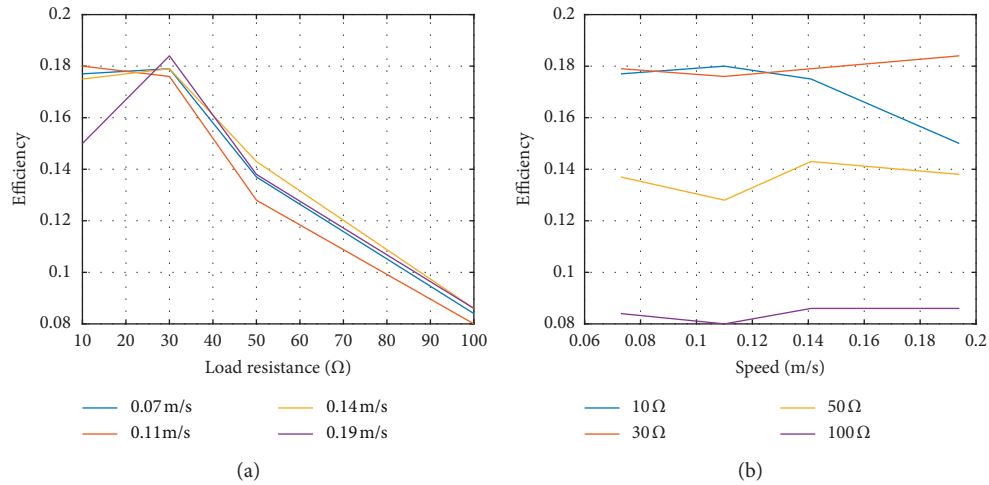

Figure 10: Variation of efficiency with (a) speed and (b) load resistance.

thus, the rationality of the simulation model is verified. (2) Actual test load power and efficiency differ from those in the simulation at the same speed and same load resistance conditions. This is because the simulation is performed based on ideal conditions, whereas in the actual situation, the low oil temperature, the effect of the pipeline layout, and the actual power generation characteristics of the generator affect the recovery power and efficiency. (3) With increasing excitation speed and decreasing external load resistance, the extension stroke feed power increases significantly. (4) Because the excitation speed affects both inherent damping force and overall damping force, the feed efficiency is not affected by the excitation speed but greatly affected by the external load resistance. That is, as the load resistance decreases, the feed efficiency increases drastically. (5) The generator selected for the prototype has a rated power of 100 W, which has low power-generation efficiency under large load and large speed and stable power generation at the rated power. This causes a significant inflection point in the efficiency plots.

7. Conclusions

In this study, a hydraulic shock absorber was proposed, and the design principle and mathematical model were described in detail. The principle prototype was built to verify the damping characteristics and energy recovery characteristics. The main conclusions are as follows:

(1) The controllable range of the damping force depends on the external load and excitation frequency. To obtain an asymmetrical extension/compression damping force, the controllable range of the extension stroke is large. At an excitation frequency of 0.62 Hz, the external load ranged from 10 to 100 Ω, and the peak damping force ranged from −3393 to −2210 N.

(2) The simulation results indicate that, under the target damper characteristics, the peak recovery power of the energy-absorbing damper was 505.52 W, and the recovery efficiency was 14.5%.

(3) Energy recovery power depends on the excitation speed and external load. At an excitation speed of 0.19 m/s and external load of 10 Ω, the recovered power was 103.7 W. The energy recovery efficiency mainly depends on the external load. At varying external load, the recovery efficiency ranged from 8% to 18%, whereas at varying excitation speed, the efficiency fluctuated by only 2%.

Data Availability

The authors declare that all data sources are original.

Conflicts of Interest

The authors declare no conflicts of interest.

Authors' Contributions

Zhifei Wu contributed to methodology and Guangzhao Xu was responsible for validation. All authors have read and approved the final manuscript.

Acknowledgments

This research was funded by The Shanxi Province Science and Technology Major Project, grant number: 20181102006. The authors are grateful for the support by the Vehicle Department of Taiyuan University of Technology.

References

[1] J. Ruan, P. Walker, and N. Zhang, "A comparative study energy consumption and costs of battery electric vehicle transmissions," *Applied Energy*, vol. 165, pp. 119–134, 2016.

[2] C. Fiori, K. Ahn, and H. A. Rakha, "Power-based electric vehicle energy consumption model: model development and validation," *Applied Energy*, vol. 168, pp. 257–268, 2016.

[3] W. Salman, L. Qi, X. Zhu et al., "A high-efficiency energy regenerative shock absorber using helical gears for powering low-wattage electrical device of electric vehicles," *Energy*, vol. 159, pp. 361–372, 2018.

[4] R. Zhang and X. Wang, "Parameter study and optimization of a half-vehicle suspension system model integrated with an arm-teeth regenerative shock absorber using Taguchi method," *Mechanical Systems and Signal Processing*, vol. 126, pp. 65–81, 2019.

[5] L. Zuo, B. Scully, J. Shestani, and Y. Zhou, "Design and characterization of an electromagnetic energy harvester for vehicle suspensions," *Smart Materials and Structures*, vol. 19, no. 4, p. 45003, 2010.

[6] X.-c. Zheng, F. Yu, and Y.-c. Zhang, "A novel energy-regenerative active suspension for vehicles," *Journal of Shanghai Jiaotong University (Science)*, vol. 13, no. 2, pp. 184–188, 2008.

[7] G. Zhang, J. Cao, and F. Yu, "Design of active and energy-regenerative controllers for DC-motor-based suspension," *Mechatronics*, vol. 22, no. 8, pp. 1124–1134, 2012.

[8] S. Li, J. Xu, X. Pu, T. Tao, H. Gao, and X. Mei, "Energy-harvesting variable/constant damping suspension system with motor based electromagnetic damper," *Energy*, vol. 189, p. 116199, 2019.

[9] J. A. Stansbury III, "Regenerative suspension with accumulator systems and methods," U.S. Patent 7,938,217, 2011.

[10] A. Okamoto, "Energy regeneration device for either hybrid vehicle or electric automobile," U.S. Patent 8,479,859, 2013.

[11] S. Carabelli, A. Tonoli, A. Festini et al., "Suspension system for a wheeled vehicle and a wheeled vehicle equipped with such a suspension system," U.S. Patent 7,942,225, 2011.

[12] Z. G. Fang, X. X. Guo, and L. Zuo, "Potential study and sensitivity analysis of energy regenerative suspension," *Journal of Jiangsu University*, vol. 34, pp. 373–377, 2013.

[13] L. Xu, "Structure designs and evaluation of performance simulation of hydraulic transmission electromagnetic energy-regenerative active suspension," in *SAE Technical Paper Series*, SAE International, Warrendale, PA, USA, 2011.

[14] Z. Fang, X. Guo, L. Xu, and H. Zhang, "Experimental study of damping and energy regeneration characteristics of a hydraulic electromagnetic shock absorber," *Advances in Mechanical Engineering*, vol. 5, Article ID 943528, 2013.

[15] Z. Fang, X. Guo, L. Xu, and H. Zhang, "An optimal algorithm for energy recovery of hydraulic electromagnetic energy-regenerative shock absorber," *Applied Mathematics and Information Sciences*, vol. 7, no. 6, pp. 2207–2214, 2013.

[16] M. A. A. Abdelkareem, L. Xu, M. K. A. Ali et al., "Vibration energy harvesting in automotive suspension system: a detailed review," *Applied Energy*, vol. 229, pp. 672–699, 2018.

[17] J. Zou, X. Guo, L. Xu et al., "Simulation research of a hydraulic interconnected suspension based on a hydraulic energy regenerative shock absorber," in *SAE Technical Paper Series*, SAE International, Warrendale, PA, USA, 2018.

[18] J. Zou, X. Guo, M. A. A. Abdelkareem, L. Xu, and J. Zhang, "Modelling and ride analysis of a hydraulic interconnected suspension based on the hydraulic energy regenerative shock absorbers," *Mechanical Systems and Signal Processing*, vol. 127, pp. 345–369, 2019.

[19] M. A. A. Abdelkareem, L. Xu, X. Guo et al., "Energy harvesting sensitivity analysis and assessment of the potential power and full car dynamics for different road modes," *Mechanical Systems and Signal Processing*, vol. 110, pp. 307–332, 2018.

[20] M. A. A. Abdelkareem, L. Xu, M. K. A. Ali et al., "On-field measurements of the dissipated vibrational power of an SUV car traditional viscous shock absorber," in *Proceedings of the ASME 2018 International Design Engineering Technical Conferences and Computers and Information in Engineering Conference*, American Society of Mechanical Engineers (ASME), Quebec City, Canada, August 2018.

[21] M. A. A. Abdelkareem, L. Xu, M. K. A. Ali et al., "Analysis of the prospective vibrational energy harvesting of heavy-duty truck suspensions: a simulation approach," *Energy*, vol. 173, pp. 332–351, 2019.

[22] Z. Wu, Y. Xiang, M. Li, M. Y. Iqbal, and G. Xu, "Investigation of accumulator main parameters of hydraulic excitation system," *Journal of Coastal Research*, vol. 93, no. sp1, pp. 613–622, 2019.